TOXICOLOGICAL SCIENCES **135(1)**, 48–62 2013
doi:10.1093/toxsci/kft124
Advance Access publication June 6, 2013

Impact of Pregnancy on the Pharmacokinetics of Dibenzo[def,p]chrysene in Mice

Susan Ritger Crowell,*[,1] Arun K. Sharma,† Shantu Amin,† Jolen J. Soelberg,* Natalie C. Sadler,* Aaron T. Wright,* William M. Baird,‡ David E. Williams,‡ and Richard A. Corley*

*Fundamental and Computational Sciences Directorate, Pacific Northwest National Laboratory, Richland, Washington 99352; †Department of Pharmacology, Penn State University College of Medicine, Hershey, Pennsylvania 17033; and ‡Department of Environmental and Molecular Toxicology, Oregon State University, Corvallis, Oregon 97331

[1]To whom correspondence should be addressed at Systems Toxicology, 902 Battelle Boulevard, Richland, WA 99352. Fax: 509-371-6978. E-mail: susan.crowell@pnnl.gov.

Received March 27, 2013; accepted May 24, 2013

Polycyclic aromatic hydrocarbons (PAHs) are ubiquitous environmental contaminants generated during combustion. Dibenzo[def,p]chrysene (DBC) is a high molecular weight PAH classified as a 2B carcinogen by the International Agency for Research on Cancer. DBC crosses the placenta in exposed mice, causing carcinogenicity in offspring. We present pharmacokinetic data of DBC in pregnant and nonpregnant mice. Pregnant (gestational day 17) and nonpregnant female B6129SF1/J mice were exposed to 15 mg/kg DBC by oral gavage. Subgroups of mice were sacrificed up to 48 h postdosing, and blood, excreta, and tissues were analyzed for DBC and its major diol and tetrol metabolites. Elevated maximum concentrations and areas under the curve of DBC and its metabolites were observed in blood and tissues of pregnant animals compared with naïve mice. Using a physiologically based pharmacokinetic (PBPK) model, we found observed differences in pharmacokinetics could not be attributed solely to changes in tissue volumes and blood flows that occur during pregnancy. Measurement of enzyme activity in naïve and pregnant mice by activity-based protein profiling indicated a 2- to 10-fold reduction in activities of many of the enzymes relevant to PAH metabolism. Incorporating this reduction into the PBPK model improved model predictions. Concentrations of DBC in fetuses were one to two orders of magnitude below maternal blood concentrations, whereas metabolite concentrations closely resembled those observed in maternal blood.

Key Words: **PBPK modeling; dibenzo[def,p]chrysene; polycyclic aromatic hydrocarbons; pregnancy; gestation.**

Dibenzo[def,p]chrysene (DBC; formerly referred to as dibenzo[a,l]pyrene) is a six-ringed polycyclic aromatic hydrocarbon (PAH) observed to be highly carcinogenic in laboratory animals. Specifically, DBC exposure has been shown to cause skin tumors in SENCAR mice exposed dermally (Cavalieri *et al.*, 1989, 1991; Higginbotham *et al.*, 1993; Lavoie *et al.*, 1993), mammary tumors in Sprague Dawley rats exposed intramammarily (Cavalieri *et al.*, 1991), and lung and liver cancers in CD-1 and A/J mice exposed ip (Platt *et al.*, 2004; Prahalad *et al.*, 1997). DBC has been found to be approximately 100-fold more potent in producing lung adenomas than benzo[a]pyrene (B[a]P) (Prahalad *et al.*, 1997). The International Agency for Research on Cancer (IARC) currently classifies DBC as a 2B or possibly carcinogenic to humans (IARC, 2010).

DBC is a persistent environmental contaminant because of its high lipophilicity (log K_{OW} = 7.2), negligible volatility, and high molecular weight. In mammalian systems, DBC undergoes complex metabolism centering upon the reactive fjord region, with diol epoxide and *o*-quinone metabolites as the primary carcinogenic metabolites (Xue and Warshawsky, 2005). As with B[a]P, CYP1A1 and CYP1B1 are the primary oxidizers of DBC (Buters *et al.*, 2002). CYP1B1 is constitutively expressed in lung and a variety of hormonal tissues (e.g., adrenal, thymus, ovary, testes, and mammary glands) and is also inducible in liver tissue, whereas CYP1A1 has low constitutive expression and high inducibility in hepatic and extrahepatic tissues (Buesen *et al.*, 2002; Walker *et al.*, 1995; Zhang *et al.*, 2003).

Recently, DBC has been shown to cross the placenta in B6129SF1/J mice, causing T-cell lymphoma, lung adenoma, and liver lesions in offspring of mothers exposed to single doses of 15 mg/kg DBC on gestation day 17 (Castro *et al.*, 2008a; Yu *et al.*, 2006). Although subsequent studies have focused on the impact of dose and timing of maternal exposure (Castro *et al.*, 2008b; Shorey *et al.*, 2012) and the metabolic basis of disease in the developing fetus (Castro *et al.*, 2008a), there has been no prior focus on the impact of pregnancy itself on the disposition of DBC and its metabolites.

In this study, we sought to examine the pharmacokinetics of DBC and its hydroxylated metabolites in B6129SF1/J mice during late pregnancy compared with the naïve adult female

mouse, as well as to establish the presence and pharmacokinetics of DBC in the developing fetus. To explore potential mechanisms involved in the differences observed in pharmacokinetics between pregnant and naïve animals, a previously published physiologically based pharmacokinetic (PBPK) model of DBC disposition (Crowell *et al.*, 2011) was extended to include pregnancy and the developing fetus. *In vitro* metabolic rates were determined in liver microsomes of adult female mice using traditional methods. Additionally, to assess changes in metabolism during pregnancy, enzyme activities in hepatic microsomes from naïve and pregnant mice were measured by activity-based protein profiling (ABPP), a chemical probe-dependent chemoproteomic approach that requires the catalytic activity of P450 enzymes to generate a measurable signal by liquid chromatography-mass spectrometry (LC-MS)-based proteomics or fluorescence to directly report on P450 functional activity.

MATERIALS AND METHODS

Reagents and Chemicals

DBC, DBC-11,12-diol, and DBC-11,12,13,14-tetraols were synthesized according to previously reported methods (Krzeminski *et al.*, 1994; Luch *et al.*, 1998; Sharma *et al.*, 2004). B[a]P (for use as an internal standard), sodium sulfate, sulfuric acid, acetone, methanol, tetrahydrofuran, ethyl acetate, and NADPH were purchased from Sigma (St Louis, MO). All solvents were of high-performance liquid chromatography (HPLC) grade.

Highly concentrated PAH stocks of B[a]P and DBC were diluted with acetone to create working solutions with ranges of concentrations from 0.01 to 2.5mM, for use as analytical and internal standards and substrates in metabolism assays. Solutions were stored at −80°C in amber vials wrapped with parafilm to prevent degradation or evaporation. Theoretical stock concentrations were confirmed by HPLC with fluorescence detection.

Animals

Female B6129SF1/J and male 129S1/Svlmj mice (Jackson Laboratory, Bar Harbor, ME) were housed separately in suspended plastic cages with chipped bedding, in rooms maintained at 21°C ± 2°C and 50 ± 10% relative humidity with a 12-h light/dark cycle. Mice were given a minimum acclimation period of 7 days before experiments were begun. Lab diet certified rodent chow and water were provided *ad libitum*. The animal facility is accredited by the American Association for Accreditation of Laboratory Animal Care. All animal protocols were approved by the Institutional Animal Care and Use Committee at Pacific Northwest National Laboratory and studies were performed in accordance with the National Institutes of Health (NIH) guidelines for the care and use of laboratory animals (NIH, 2011).

In Vitro *Metabolism Studies*

Hepatic microsomes were prepared according to the methods of Guengerich (1994). Briefly, adult female B6129SF1/J mice were euthanized by CO_2 asphyxiation followed by exsanguination, and liver tissue excised. Tissue was immediately placed in ice-cold 0.1M PBS (pH 7.4). Livers were subsequently weighed and placed in 2 ml/g tissue of homogenization buffer (1M Tris-acetate, pH 7.4; 1M KCl; 100mM EDTA), and homogenized by 6–8 passes of a drill press. Homogenate was centrifuged at 4°C, 10,000 × g, for 30 min. The S9 fraction was decanted, and centrifuged for an additional 60 min at 4°C and 105,000 × g. Supernatant (cytosolic fraction) was decanted and stored at −80°C. Wash buffer (100mM K pyrophosphate; 100mM EDTA) was added to the ultracentrifuge tube to dislodge the pellets (microsomal fraction), which were then pooled and centrifuged a final time for 45 min at 4°C and 105,000 × g. Supernatant was discarded and the pellets resuspended at 0.5 ml/g original tissue weight of resuspension buffer (1M Tris-acetate; 100mM EDTA). Microsomes were aliquoted by 0.5 ml volumes and stored at −80°C until use. Microsomal protein (MSP) concentration was determined by bicinchoninic acid spectrophotometric assay, using bovine serum albumin as a standard of known concentration. A CO difference spectrum assay was used to determine the microsomal CYP450 enzyme content.

Reactions were conducted in 500 µl total volumes, consisting of 0.1M phosphate buffer (pH 7.4), MSP (0.25–1.0 mg/ml), $MgCl_2$ (3mM), and excess NADPH (1.5mM). Reactions were initiated by the addition of DBC dissolved in an acetone vehicle (total organic in reaction less than 1% vol/vol) to a final reaction concentration of 0.03–9.0µM and were incubated at 37°C for 0–20 min. Control experiments were performed to verify that reaction kinetics were linear with regard to time and MSP content, and without key substrates to establish baseline chromatography (without DBC) and substrate stability over time (without NADPH). Reactions were quenched with the addition of 500 µl 0.9M H_2SO_4, followed by the addition of a 5 µl B[a]P internal standard. Samples were then vortexed and placed on ice until extraction.

Liquid-liquid extractions were performed on metabolism samples as follows: 250 mg Na_2SO_4 was added to each sample, followed by 500 µl ethyl acetate. Samples were vortexed, and then centrifuged for 10 min at 4°C and 1600 × g. The supernatant was drawn off using glass Pasteur pipettes to a new tube, and then the extraction was repeated. The combined supernatants were blown to dryness under a gentle stream of nitrogen. Samples were reconstituted in 500 µl methanol and analyzed as described below.

Initial reaction velocity (V, µM/min) was obtained by linear regression of PAH concentration depletion over time from individual kinetic experiments. In order to determine metabolic kinetic parameters, nonlinear regression of protein normalized initial velocities versus initial reaction substrate concentration ([S], µM) was performed using R: A Language and Environment for Statistical

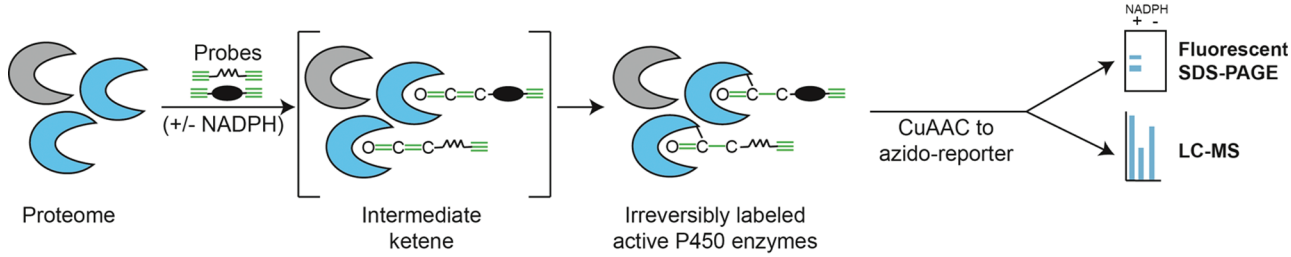

FIG. 1. A proteome sample containing active cytochrome P450 enzymes is treated with two chemical probes developed from known mechanism-based inhibitors of P450s. Each probe contains an alkyne for reaction with the catalytic machinery of the enzyme and a second alkyne for CuAAC. In the presence of NADPH, reactive P450s oxidize a probe alkyne to a reactive ketene, which in turn acts as an electrophile and irreversibly reacts with a nucleophilic moiety within the P450 active site. Using CuAAC, reporter groups can be appended for downstream measurement of probe-labeled proteins, for example, an azido-tetramethylrhodamine for fluorescent imaging, or an azido-biotin for subsequent streptavidin-mediated enrichment and LC-MS analysis.

Computing Version 2.13.1 (R Foundation for Statistical Computing, Vienna, Austria) according to the Michaelis-Menten model:

$$V_S = \frac{V_{MAX}[S]}{K_M + [S]}, \quad (1)$$

where V_{MAX} (nmol/min/mg MSP) is the maximum enzyme velocity and K_M (μM) is the Michaelis constant, defined as the initial reaction concentration required to reach half the V_{MAX}.

Pharmacokinetic Studies

Design. We performed two pharmacokinetic studies of DBC in B6129SF1/J mice: (1) naïve adult females and (2) pregnant females. For the latter, mice were bred with 129S/SvImj males after the 1-week acclimation period. The appearance of a vaginal plug was designated gestational day (gd) 0, and DBC exposures occurred on gd 17 as in previous studies (Castro *et al.*, 2008a; Yu *et al.*, 2006).

Naïve ($n = 36$, 19.9 ± 0.9 g body weight) and pregnant ($n = 36$, 35.6 ± 3.0 g body weight) female mice were administered 15 mg/kg DBC in corn oil by oral gavage (0.2 ml/kg body weight), as in previous studies (Crowell *et al.*, 2011; Yu *et al.*, 2006). At 0.5, 1, 1.5, 2, 2.5, 3, 3.5, 4, 6, 12, 24, and 36 (pregnant) or 48 (naïve) h postexposure, subgroups of three mice were sacrificed by CO_2 asphyxiation followed by exsanguination through the inferior vena cava. The duration of the pharmacokinetic study in pregnant mice was reduced from the originally planned 48 to 36 h due to earlier than expected (based upon prior studies) delivery of several litters. Animals designated for 36 and 48 h sacrifice were individually housed in all-glass metabolism cages for separate collection of urine and feces over dry ice at 0–12, 12–24, and 24–36 (pregnant) or 24–48 (naïve) h postdosing. Whole blood was collected in heparinized glass vials. Gastrointestinal tissues were manually separated from their contents and rinsed with water; contents and rinsate were saved. All samples were flash frozen and stored at −80°C until analyses.

Genotyping of offspring. As described in Castro *et al.* (2008a) and Yu *et al.* (2006), offspring of the B6129SF1/J × 129S/SvImj cross are approximately half AHR-responsive ($AHR^{b\text{-}1/d}$) and half AHR-nonresponsive ($AHR^{d/d}$) genotypes with AHR responsiveness being a susceptibility factor for carcinogenicity. At necropsy, tail clips were collected, flash frozen in liquid nitrogen, and stored at −80°C until genotyping. Tail clips were lysed overnight at 55°C in 200 μl of Direct PCR Lysis Reagent (Viagen Biotech Inc., Los Angeles, CA) containing 60 μg proteinase K (Life Sciences, Tech., Carlsbad, CA), followed by heat inactivation of proteinase K for 45 min at 85°C. The resulting lysate was briefly centrifuged prior to undergoing a 10 μl PCR reaction containing 1 μl lysate template, 1× Biolase buffer, 2.5mM $MgCl_2$, 1 U Biolase polymerase (Bioline USA Inc., Taunton, MA), 0.2mM each dNTPs (Fermentas, Glen Burnie, MD), 0.4μM each 5′-gaagcatgcagaacgaggag common forward primer, 5′-gaagcatgcagaacgaggag $AHR^{d/d}$ reverse primer, and 0.2μM 5′-caagcttatatgctg gcaagccgagttcag $AHR^{b\text{-}1/d}$ reverse primer to permit one-tube genotyping of the AHR alleles as previously described. PCR products were separated and visualized on Novex 8% Tris-borate-EDTA gels. AHR responsiveness was confirmed by the presence of two PCR products of 158 bp (b-1 allele) and 148 bp (d allele). Nonresponsive mice had a single product of 148 bp. A Gene Ruler 100 bp Plus ladder (Fermentas) was included on each gel, and ethidium bromide was used to stain the DNA, followed by UV visualization.

Sample Analysis

Pharmacokinetic study samples were prepared for analysis as follows. For blood, 250 mg whole blood were spiked with 5 μl of an 8.6μM B[a]P solution as an internal standard. Two hundred and fifty microliters of 0.9M H_2SO_4 and 250 mg Na_2SO4 were added to each sample and vortexed for 30 s. For excreta and tissues other than blood, 100–250 mg material was homogenized without the addition of H_2SO_4 (Na_2SO_4 still added) using a Tissue Tearor or, in the case of lung, finely minced with a razor blade and was then spiked with 5 μl of an 8.6μM B[a]P solution as an internal standard and vortexed well. For urine and

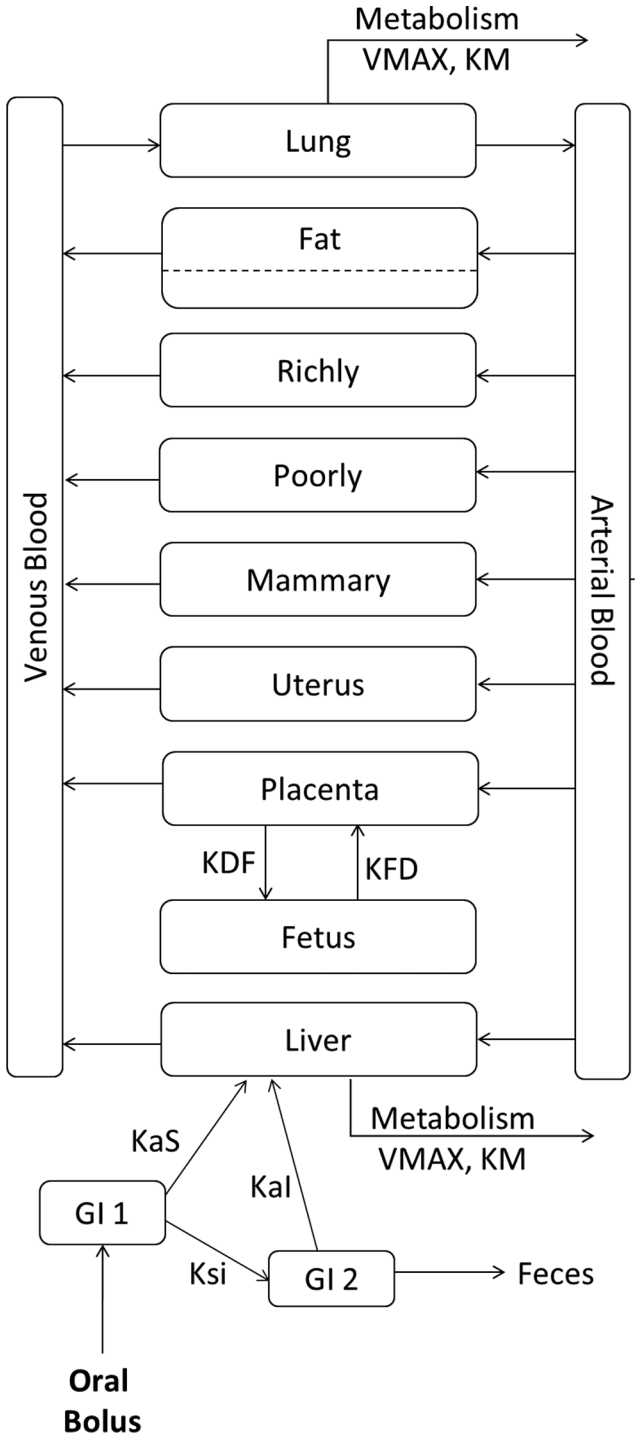

FIG. 2. Schematic of DBC PBPK model in mice. DBC is administered via oral gavage via a two-compartment theoretical GI tract. Subsequent to exposure and uptake, DBC moves between physiological compartments (blood, lung, fat, liver, richly and poorly perfused tissues, mammary glands, uterus, and in pregnant animals, lumped placentas and lumped fetuses) based on blood flow rates and concentrations, and in the case of fat, tissue permeability. Saturable metabolism occurs in liver and lung compartments. Tables 1 and 2 provide a list of model parameter definitions and values.

TABLE 1
Physiological Parameters for DBC PBPK Model

Parameter	Symbol	Naïve	GD 17
Body weight[a] (g)	BW	19.9 ± 0.9	36.6 ± 3.0
Average litter size[a]	NUMFET	—	7.82 ± 2.0
Cardiac output (ml/min)	QCC	1.253	1.188[b]
Fractional tissue volumes (% body weight, unitless)			
Arterial blood	VARTC	0.017	0.0097[c]
Venous blood	VVENC	0.033	0.0189[c]
Fat	VFATC	0.07	0.0561[d]
Blood in fat (% of fat volume)	VFATBLDC	0.02	0.02
Liver	VLIVC	0.055	0.0418[c]
Lung	VLNGC	0.0073	0.0042[c]
Uterus	VUTC	0.002	0.0114[d]
Mammary glands	VMAMC	0.01	0.0401[d]
Placenta	VPLAC	—	0.00361[d,e]
Fetus	VFETC	—	0.0313[d,e]
Poorly perfused tissues	VPOORC	0.55	0.343[c]
Richly perfused tissues[f]	VRICHC	0.156	0.101
Fractional blood flows (% cardiac output)			
Fat	QFATC	0.07	0.068[g]
Liver	QLIVC	0.161	0.149[g]
Uterus	QUTC	0.005	0.035[g]
Mammary glands	QMAMC	0.002	0.01[g]
Placenta	QPLA1C	—	0.029[d,e]
Poorly perfused tissues	QPOORC	0.217	0.217
Richly perfused tissues[h]	QRICHC	0.545	0.294

Note. [a]Study specific values.
[b]QCgd17 = QC + ∑(QTgd17 − QT), as described in O'Flaherty *et al.* (1992).
[c]Static compartments—no change in absolute volume from naïve mouse (O'Flaherty *et al.*, 1992).
[d]Growth compartment (O'Flaherty *et al.*, 1992).
[e]Individual conceptus value.
[f]0.9 − (VPoorC + VTissC).
[g]Change in relative blood flow calculated as a function of change in compartment volume. QTgd17 = QT(VTgd17/VT) (O'Flaherty *et al.*, 1992).
[h]1.0 − (QPoorC + QTissC).

feces, samples were prepared with and without treatment with β-glucuronidase (100 units/sample or 0.4–1.0 units/mg) at 37°C for 22 h.

All pharmacokinetic study samples were then thrice extracted with 0.5 ml ethyl acetate and centrifuged for 10 min at 1400 × g, and the combined supernatant of each sample evaporated to dryness under a gentle stream of nitrogen. Samples were reconstituted in 100 µl methanol for analysis.

For both *in vitro* metabolism and pharmacokinetic study samples, DBC, DBC diol and tetraol metabolites, and B[a]P internal standards were quantitated by reverse-phase HPLC using an Agilent 1100 HPLC system equipped with an Agilent 1100 variable wavelength fluorescence detector (Santa Clara, CA). Twenty microliters of reconstituted sample were injected onto an Ascentis 25 cm × 4.6 mm, 5 µm C18 column (Sigma-Aldrich, St Louis, MO). A water:acetonitrile gradient from 45:55 to 0:100 was employed from 0 to 10 min, and then held at 100% acetonitrile until 22 min, at a constant flow rate of 0.95 ml/min. Excitation and emission wavelengths were 245 and 430 for DBC-11,12,13,14-tetraols, and 360 and 430 for DBC-11,12-diol, and 235 and 430 for B[a]P and DBC. Elution times were 5.5, 6.1, and 6.6 min for DBC-11,12,13,14-tetraols, 10.4 min for DBC-11,12-diol, 16.6 min for B[a]P, and 19.0 min for DBC. Limits of reliable quantitation were typically on the order of 1–8 ng/g for DBC and DBC-11,12-diol and 5–20 ng/g for DBC-11,12,13,14-tetraols in each of the biological matrices.

Activity-Based Protein Profiling

ABPP utilizes chemical probes derived from mechanism-based inhibitors of P450 enzymes to directly report upon the activity of P450 enzymes in one or more samples. Herein, we utilize an arylalkyne (2EN-ABP, Wright and Cravatt, 2007) or aliphatic alkyne (probe 5 in Wright *et al.*, 2009) containing chemical probe. Arylalkyne and aliphatic alkynes are known mechanism-based inhibitors of P450 enzymes (Hollenberg *et al.*, 2008). As illustrated in Figure 1, the chemical probes are oxidized directly by P450 enzymes in a NADPH-dependent manner to yield a reactive ketene moiety on the probe. The electrophilic ketene then reacts irreversibly with a nucleophilic amino acid residue within the active site of the P450, providing a covalent handle for downstream analyses. Each probe also contains a second alkyne group that permits a copper-catalyzed azide-alkyne cycloaddition to append fluorescent reporters for gel imaging or biotin for enrichment and LC-MS analyses (Wright and Cravatt, 2007). Due to broad substrate specificity of many P450 enzymes, particularly those associated with detoxification and phase I metabolism, the utilization of two probes permits a greater breadth of measurement coverage of P450 activity.

Microsomal proteome (1 mg/ml protein concentration) samples were treated with a mixture of the two activity-based probes (ABPs). Control samples were prepared by heat-shock pretreatment of the microsome samples (98°C, 8 min) prior to addition of ABPs and NADPH. Following ABP incubation, the samples were reacted with a biotin-azide tag under click-chemistry conditions (Ansong *et al.*, 2013; Speers *et al.*, 2003). ABP-labeled proteins were enriched on streptavidin resin, reduced with tris(2-carboxyethyl)phosphine (TCEP), and alkylated with iodoacetamide (Ansong *et al.*, 2013). Proteins were digested on-resin with trypsin, and the resulting peptides were collected and analyzed by LC-MS as described previously (Ansong *et al.*, 2013).

Generated MS/MS spectra were searched using the SEQUEST algorithm (Yates *et al.*, 1995) against the publicly available *Mus musculus*–translated genome sequence (www.uniprot.org), and rescored using the MS-GF approach

TABLE 2
Biochemical Parameters for DBC PBPK Model

Parameter	Symbol	Units	Value
Partition coefficients			
Fat	PFATP	—	496.56[a]
Liver	PLIVP	—	13.32[a]
Lung	PLNGP	—	7.49[a]
Uterus	PUTP	—	13.32[b]
Mammary glands	PMAMP	—	13.32[b]
Placenta	PPLAP	—	13.32[b]
Poorly perfused tissues	PPOORP	—	12.11[a]
Richly perfused tissues	PRICHP	—	13.32[a]
Fractional binding in blood	FB	—	0.9[a]
Fat permeation coefficient	PAFATPC	—	0.25[a]
Absorption rate from stomach	KAS	1/min	0.0001[c]
Absorption rate from intestines	KAI	1/min	0.0035[c]
Gastric emptying rate	KSI	1/min	0.016[d]
Fecal elimination rate	KIF	1/min	0.00005[e]
Placental transfer rate, dam to fetus	KDTFPC	1/min	0.02[c]
Placental transfer rate, fetus to dam	KFTDPC	1/min	0.08[c]
Maximal rate of metabolism in liver	VMAXLIVPA	nmol/min/ml	33.4[f]
Maximal rate of metabolism in lung	VMAXLNGPA	nmol/min/ml	4.43[g]
Michaelis constant for metabolism in liver	KMLIVPA	nmol/ml	7.35[f]
Michaelis constant for metabolism in lung	KMLNGPA	nmol/ml	7.35[b]

Note. Parameters were used in both nonpregnant and pregnant models.
[a]Crowell *et al.* (2011).
[b]Liver value.
[c]Optimized.
[d]Exponential regression of stomach contents data of CD-1 mice from Osinski *et al.* (2002).
[e]Visually estimated.
[f]Experimentally measured.
[g]Liver value scaled to lung.

(Kim *et al.*, 2008). Identified peptides of at least six amino acids in length having Mass spectral generating function (MS-GF) scores ≤ 1E-10, which corresponds to an estimated false discovery rate (FDR) < 1% at the peptide level, were used to generate an accurate mass and time (AMT) tag database (Zimmer *et al.*, 2006). Matched features from each LC-MS data set were then filtered on a FDR of less than or equal to 5% using the Statistical Tools for AMT tag confidence metric (Stanley *et al.*, 2011). Relative peptide abundance measurements in technical replicates were normalized to the data set with the least information using linear regression in DAnTE (Polpitiya *et al.*, 2008). Peptide abundance values were then rolled up to proteins using RRollup (Polpitiya *et al.*, 2008); a minimum of five peptides was required for the Grubb's test, with a p value cutoff of 0.05. Only peptides unique in identifying a single protein were utilized to estimate protein abundances. Additionally, proteins represented by < 2 unique peptides were removed. To identify a protein as specifically labeled by the ABPs, we required the following criteria: (1) peptide measurements for a protein exhibit a significant difference comparing ABP-labeled + NADPH with ABP-labeled minus NADPH or the heat-shock controls ($p < 0.05$) and (2) the protein exhibits ≥ 2-fold more abundance in the ABP-labeled + NADPH sample relative to the controls.

PBPK Modeling

The PBPK model employed in this work is based on a previously published model for DBC (Crowell *et al.*, 2011) that was extended in this study to include pregnancy and the developing fetus using the approach developed by O'Flaherty *et al.* (1992). The adult female model consisted of compartments representing blood, liver, fat, lung, uterus, mammary glands, and lumped richly and poorly perfused tissues; the pregnancy model contained additional compartments representing aggregated placentas and fetuses (Fig. 2). All compartments except fat were well mixed and flow limited; fat was described by diffusion-limited distribution.

Absorption of orally administered DBC occurred via a two-compartment theoretical gut (Staats *et al.*, 1991) in which first-order rate equations described absorption into the liver, transfer between gut compartments, and elimination into feces. Bioavailability was addressed through the rates of gut motility and absorption, rather than the inclusion of a fractional absorption coefficient, so that the quantity of parent DBC recovered in the feces varied dynamically based on exposure. Fractional binding of DBC in blood was described based on reports of binding for a structurally similar PAH, B[a]P (Aarstad *et al.*, 1987). Saturable metabolism (oxidation) described by the kinetic parameters V_{MAX} and K_M occurred in liver and lung compartments and was based on kinetic parameters measured as part of this work. Hepatic V_{MAX} was scaled to model units (nmol/min/ml) by means of Equation 2:

$$\text{Model } V_{MAX} = (\text{In Vitro } V_{MAX})\left(\frac{\text{g tissue weight}}{\text{1 kg body weight}}\right)\left(\frac{\text{mg MSP}}{\text{1 g tissue weight}}\right) \quad (2)$$

Model parameters are summarized in Tables 1 and 2. Physiological parameters are taken from Brown *et al.* (1997) unless otherwise noted. For the pregnancy model, parameters reflecting blood flow and compartment size at gd 17 were derived from growth equations from O'Flaherty *et al.* (1992). Tissue volumes were scaled linearly with body weight, cardiac output was scaled as (body

TABLE 3
Cumulative Excretion of DBC and Hydroxylated Metabolites in Urine and Feces of Naïve and Pregnant Mice (Percent of Administered Dose)

			Feces				Urine			
Life stage	State	Time	DBC	Diol	Tetrol	Total	DBC	Diol	Tetrol	Total
Naïve	Free	0–12 h	0.77 ± 0.26	0.15 ± 0.035	0.79 ± 0.27	1.7 ± 0.18	—	—	0.0061 ± 0.011	0.0061 ± 0.011
		12–24 h	0.91 ± 0.35	0.19 ± 0.27	1.1 ± 0.19	2.2 ± 0.14	—	—	0.0061 ± 0.011	0.0061 ± 0.011
	Total	0–12 h	0.78 ± 0.33	0.11 ± 0.02	0.29 ± 0.04	1.2 ± 0.29	0.00043 ± 0.00042	0.013 ± 0.011	5.6 ± 4.2	5.6 ± 4.2
		12–24 h	0.90 ± 0.34	0.14 ± 0.02	0.37 ± 0.05	1.4 ± 0.30	0.00047 ± 0.00039	0.015 ± 0.010	7.0 ± 3.7	7.0 ± 3.7
Pregnant	Free	0–12 h	1.2 ± 1.0	0.098 ± 0.051	0.25 ± 0.27	1.5 ± 1.2	0.00062 ± 0.00044	0.00047 ± 0.00064	—	0.0011 ± 0.0011
		12–24 h	2.2 ± 1.3	0.28 ± 0.11	0.87 ± 0.31	3.3 ± 1.3	0.00051 ± 0.00068	0.00055 ± 0.00064	0.080 ± 0.011	0.081 ± 0.013
		24–36 h	2.2 ± 1.3	0.32 ± 0.11	1.0 ± 0.40	3.5 ± 1.3	0.0010 ± 0.00011	0.0011 ± 0.00018	0.70 ± 0.97	0.71 ± 0.97
	Total	0–12 h	1.8 ± 1.5	0.08 ± 0.03	0.10 ± 0.05	1.9 ± 1.6	0.00072 ± 0.00045	0.0067 ± 0.0048	2.8 ± 2.7	2.8 ± 2.7
		12–24 h	2.0 ± 1.5	0.16 ± 0.07	0.25 ± 0.14	2.4 ± 1.5	0.00066 ± 0.00094	0.012 ± 0.013	4.8 ± 6.0	4.9 ± 4.3
		24–36 h	2.1 ± 1.4	0.18 ± 0.07	0.30 ± 0.15	2.6 ± 1.5	0.0013 ± 0.00035	0.026 ± 0.022	10.6 ± 7.8	10.7 ± 8.3

Note. Free vs. total: total samples treated with β-glucuronidase as described in Materials and Methods. —: none detected.

weight)$^{0.75}$, and tissue perfusion rates were set as a fractions of cardiac output. Although most chemical specific parameters are those used in the preliminary DBC model (Crowell *et al.*, 2011), several parameter values were updated as additional pharmacokinetic data for DBC has been collected. Parameters describing absorption from stomach and intestines, and elimination by feces were estimated using AcslX (Aegis Corporation, Huntsville, AL) parameter estimation and visual fitting to pharmacokinetic data for DBC in blood and feces of naïve mice. Chemical specific parameters were the same in both the nonpregnancy and pregnancy models, unless otherwise noted.

Software, algorithms, and model code. The PBPK model for DBC was developed using AcslX as a system of algebraic and differential equations. The Gear algorithm was used for integration of double precision variables. Optimization of specific model parameters was achieved using the AcslX parameter estimation feature, with heteroskedasticity = 2 and the Nelder-Mead algorithm, and the fitting criterion was maximization of the log-likelihood function. Starting values for parameter estimation were determined from visual fitting of simulations to data. Model code is available upon request.

RESULTS

In Vitro *Metabolism of DBC in Naïve Mice*

Michaelis-Menten regression of metabolism data yielded a V_{MAX} of 0.81 nmol/min/mg MSP and a K_M of 7.35μM in hepatic microsomal tissue. Scaling these values to metabolic model parameters for liver and lung compartments yielded a hepatic V_{MAX} of 33.4 nmol/min/ml and pulmonary V_{MAX} of 4.43 nmol/min/ml (Table 2).

Pharmacokinetics of DBC in Naïve and Pregnant Mice

Fecal and urine excretion. Table 3 shows the cumulative excretion of DBC and metabolites in feces and urine of naïve (0–48 h, though 24–48 h samples were compromised during analysis) and pregnant (0–36 h) mice. At 24 h, pregnant animals had slightly higher levels of fecal excretion (2.4 vs. 1.4%) and lower levels of urinary excretion (4.9 vs. 7.0%) in comparison with naïve mice. Fecal excretion was primarily comprised of DBC with small quantities of conjugated hydroxylated metabolites, whereas urinary excretion was dominated by conjugated tetraol metabolites. For both naïve and pregnant animals, the low levels of parent DBC excreted in the feces at the end of each study (1.4–2.6%) indicated efficient absorption from the gastrointestinal (GI) tract following oral bolus dosing.

Directly exposed tissues: GI tract. Figure 3 displays pharmacokinetic data in small intestine of naïve and pregnant adult mice for DBC, diol, and tetraol metabolites. Pharmacokinetic analyses appear in Tables 4–6, alongside data for other tissues. Although peak concentrations of DBC and its hydroxylated metabolites were comparable or higher in naïve mice than pregnant mice (C_{MAX} ratios of 0.90, 0.97, and 0.64, respectively), those peaks occurred later in pregnant animals, and elimination tended to be slower, resulting in longer elimination half-lives and higher measures of area under the concentration curve (AUC). As the portal of entry for oral gavage administration, the peak concentrations

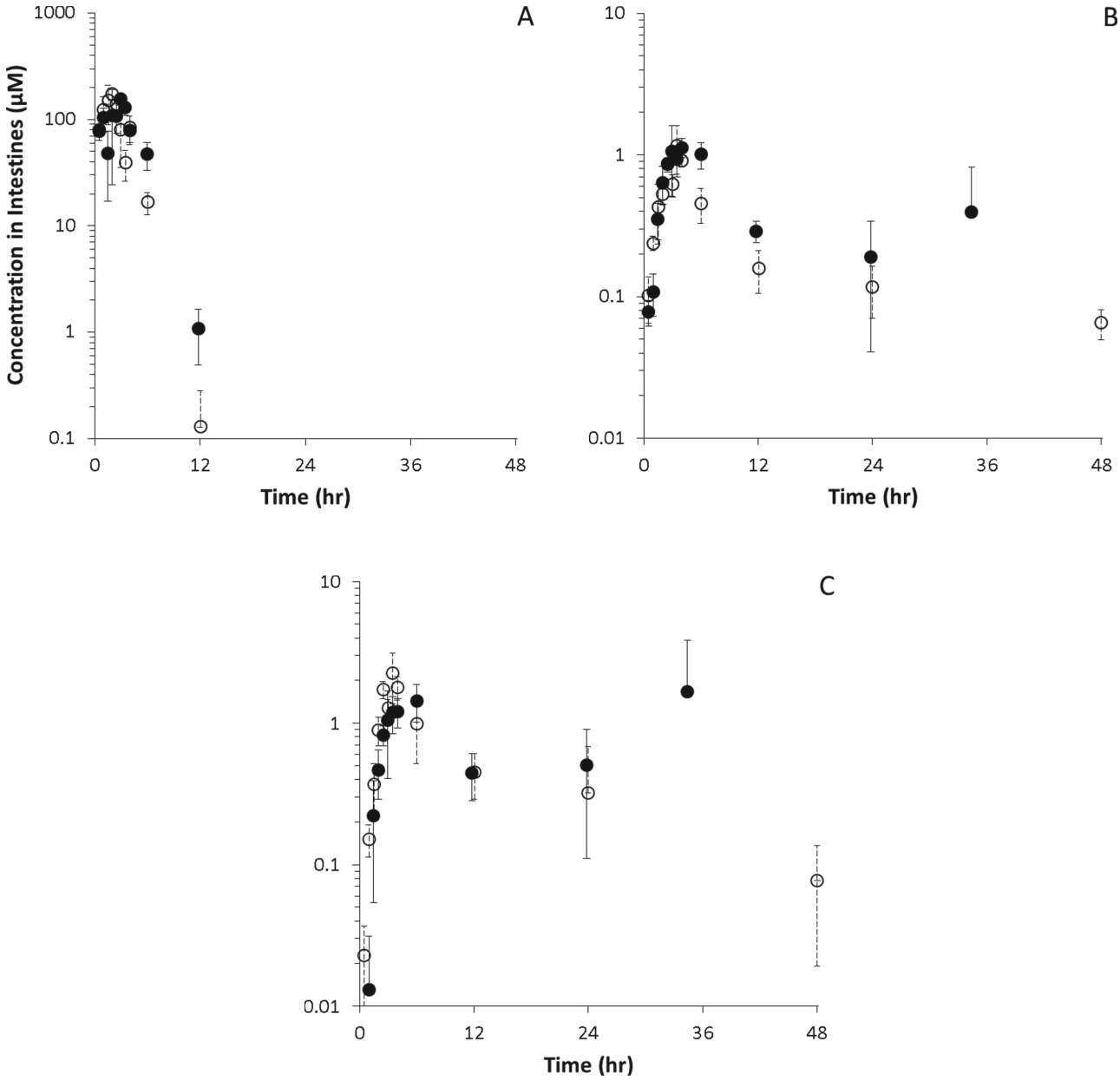

FIG. 3. DBC (A), DBC-11,12-diol (B), and DBC-11,12,13,14-tetraols (C) (µM) in small intestines of naïve (○) and pregnant (●) B6129SF1/J mice administered bolus doses of 15 mg/kg DBC in corn oil via oral gavage.

of DBC and its metabolites were significantly higher in GI than in any other tissue for both naïve and pregnant mice.

Systemically exposed tissues: blood, liver, lung, and fat. Pharmacokinetic data for systemic distribution of DBC into blood, fat, liver, and lung in naïve and pregnant mice appear in Figure 4, whereas pharmacokinetic analyses of these data appear in Table 4. Following oral bolus dosing, systemic distribution of DBC into blood and tissues was dominated by continuing absorption from the GI tract, with peak concentrations (C_{MAX}) occurring in most tissues 2–4 h subsequent to exposure (T_{MAX}). Peak concentrations in naïve mice ranged from 3.5µM in blood to 13.3µM in fat, whereas those in pregnant mice ranged from 12.9µM in blood to 17.5µM in liver. Peak concentrations of DBC were elevated in blood, liver, and lung of pregnant animals compared with naïve mice (3.72-, 3.75-, and 1.37-fold higher C_{MAX}, respectively), as were AUCs (µM·h) in these tissues (AUC ratios of 2.2, 2.8, and 1.3, respectively). Not surprisingly for a highly lipophilic chemical, peak concentrations of DBC in fat occurred 12–24 h subsequent to exposure. C_{MAX} in fat was not significantly elevated relative to the naïve mouse (1.10-fold higher C_{MAX} in pregnant mice) nor was AUC in fat (0.98). Half-lives for DBC elimination were shorter in pregnant animals in all tissues (Table 4).

Systemic distribution of DBC-11,12-diol in blood, fat, liver, and lung is shown in Figure 5, with pharmacokinetic analyses

TABLE 4
Noncompartmental Pharmacokinetic Analyses of DBC in Naïve and Pregnant Mice

Tissue		AUC (μM·h)	AUC ratio	$T_{(1/2)}$ (h)	T_{MAX} (h)	C_{MAX} (μM)	C_{MAX} ratio	% of dose	% of dose ratio
Blood	Naïve	18.8	2.36	4.8	3.5	3.46 ± 0.25	3.72	0.31 ± 0.022	2.64
	Pregnant	44.5		3.4	3.0	12.86 ± 9.63		0.83 ± 0.62	
Liver	Naïve	35.8	2.76	30.4	2.5	4.66 ± 0.26	3.75	0.46 ± 0.025	3.54
	Pregnant	98.9		5.3	4.0	17.48 ± 5.07		1.64 ± 0.52	
Lung	Naïve	79.3	1.29	6.4	2.0	12.00 ± 2.52	1.37	0.11 ± 0.023	1.42
	Pregnant	102.7		5.1	3.5	16.39 ± 1.20		0.15 ± 0.011	
Fat	Naïve	335.9	0.98	14.8	12.1	13.30 ± 2.66	1.10	1.32 ± 0.26	1.04
	Pregnant	328.0		9.8	24.0	14.60 ± 12.74		1.37 ± 1.20	
Intestine	Naïve	536.9	1.16	2.0	2.0	171.00 ± 19.67	0.90	7.82 ± 0.90	0.64
	Pregnant	620.4		2.6	3.0	153.41 ± 18.40		4.98 ± 0.60	
Placenta	Pregnant	45.8	—	8.0	3.0	5.23 ± 2.58	—	0.41 ± 0.19	—
Fetus	Pregnant	5.6	—	6.3	4.0	0.57 ± 0.097	—	0.34 ± 0.064	—

TABLE 5
Noncompartmental Pharmacokinetic Analyses of DBC-11,12-Diol in Naïve and Pregnant Mice

Tissue		AUC (μM·h)	AUC ratio	$T_{(1/2)}$ (h)	T_{MAX} (h)	C_{MAX} (μM)	C_{MAX} ratio	% of dose	% of dose ratio
Blood	Naïve	0.6	1.43	14.0	3.0	0.046 ± 0.008	2.92	0.0042 ± 0.0007	2.07
	Pregnant	0.9		7.5	2.5	0.135 ± 0.136		0.0087 ± 0.0087	
Liver	Naïve	4.0	0.78	31.9	2.5	0.382 ± 0.051	0.98	0.038 ± 0.00018	0.93
	Pregnant	3.1		9.6	3.0	0.376 ± 0.011		0.035 ± 0.0011	
Lung	Naïve	4.0	1.76	8.7	2.0	0.403 ± 0.02	1.93	0.0036 ± 0.00018	2.00
	Pregnant	7.1		5.8	3.5	0.776 ± 0.159		0.0073 ± 0.0015	
Fat	Naïve	0.5	2.46	6.6	3.0	0.081 ± 0.053	1.30	0.0081 ± 0.0053	1.22
	Pregnant	1.1		28.3	4.0	0.105 ± 0.032		0.0099 ± 0.0030	
Intestine	Naïve	9.2	1.54	21.0	3.5	1.17 ± 0.44	0.97	0.053 ± 0.020	0.69
	Pregnant	14.2		59.8	4.0	1.13 ± 0.18		0.037 ± 0.0058	
Placenta	Pregnant	3.8	—	10.6	6.0	0.361 ± 0.185	—	0.024 ± 0.0086	—
Fetus	Pregnant	2.5	—	12.4	6.0	0.16 ± 0.026	—	0.084 ± 0.016	—

TABLE 6
Noncompartmental Pharmacokinetic Analyses of DBC-11,12,13,14-Tetraols in Naïve and Pregnant Mice

Tissue		AUC (μM·h)	AUC ratio	$T_{(1/2)}$ (min)	T_{MAX} (min)	C_{MAX} (μM)	C_{MAX} ratio	% of dose	% of dose ratio
Blood	Naïve	2.6	0.43	84.5	1.0	0.088 ± 0.014	1.05	0.0079 ± 0.0013	0.75
	Pregnant	1.1		4.7	2.0	0.092 ± 0.102		0.0059 ± 0.0065	
Liver	Naïve	10.4	0.46	5.1	4.0	1.41 ± 1.22	0.58	0.14 ± 0.12	0.55
	Pregnant	4.8		5.7	3.0	0.822 ± 0.030		0.077 ± 0.028	
Intestine	Naïve	20.3	1.36	12.0	3.5	2.24 ± 0.873	0.64	0.10 ± 0.040	0.46
	Pregnant	27.6		0.9	6.0	1.44 ± 0.42		0.047 ± 0.014	

in Table 5. Peak concentrations in blood and tissues were 1–2 orders of magnitude lower than for the parent compound in both naïve and pregnant mice, ranging from 0.046μM in blood to 0.40μM in lung (naïve mice) and 0.11μM in fat to 0.78μM in lung (pregnant mice). Peak concentrations in all tissues including fat occurred between 2 and 4 h subsequent to exposure. Pregnant mice had elevated peak concentrations of DBC-11,12-diol in blood, lung, and fat (C_{MAX} ratios of 2.9, 1.9, and 1.3, respectively), whereas peak concentrations in liver were similar (0.98). AUCs followed a similar pattern, with ratios of 1.4, 1.8, and 2.4 in blood, lung, and fat, versus a ratio of 0.8 in liver.

Data for DBC-11,12,13,14-tetraols in blood and liver are shown in Figure 6, with pharmacokinetic analyses in Table 6. Tetraols in fat and lung were below limits of quantitation. Peak concentrations of tetraols were 1–2 orders of magnitude lower than for DBC in blood and were comparable between naïve and pregnant mice (0.088 and 0.092μM, respectively). Peak concentrations in liver were 3- to 20-fold lower than peak DBC concentrations and were higher in the naïve mouse relative to the pregnant mouse (1.41 vs. 0.82μM, ratio of 0.6). AUCs in blood and liver were higher in naïve animals, with ratios of pregnant:naïve of 0.43 and 0.46, respectively. The concentrations in liver

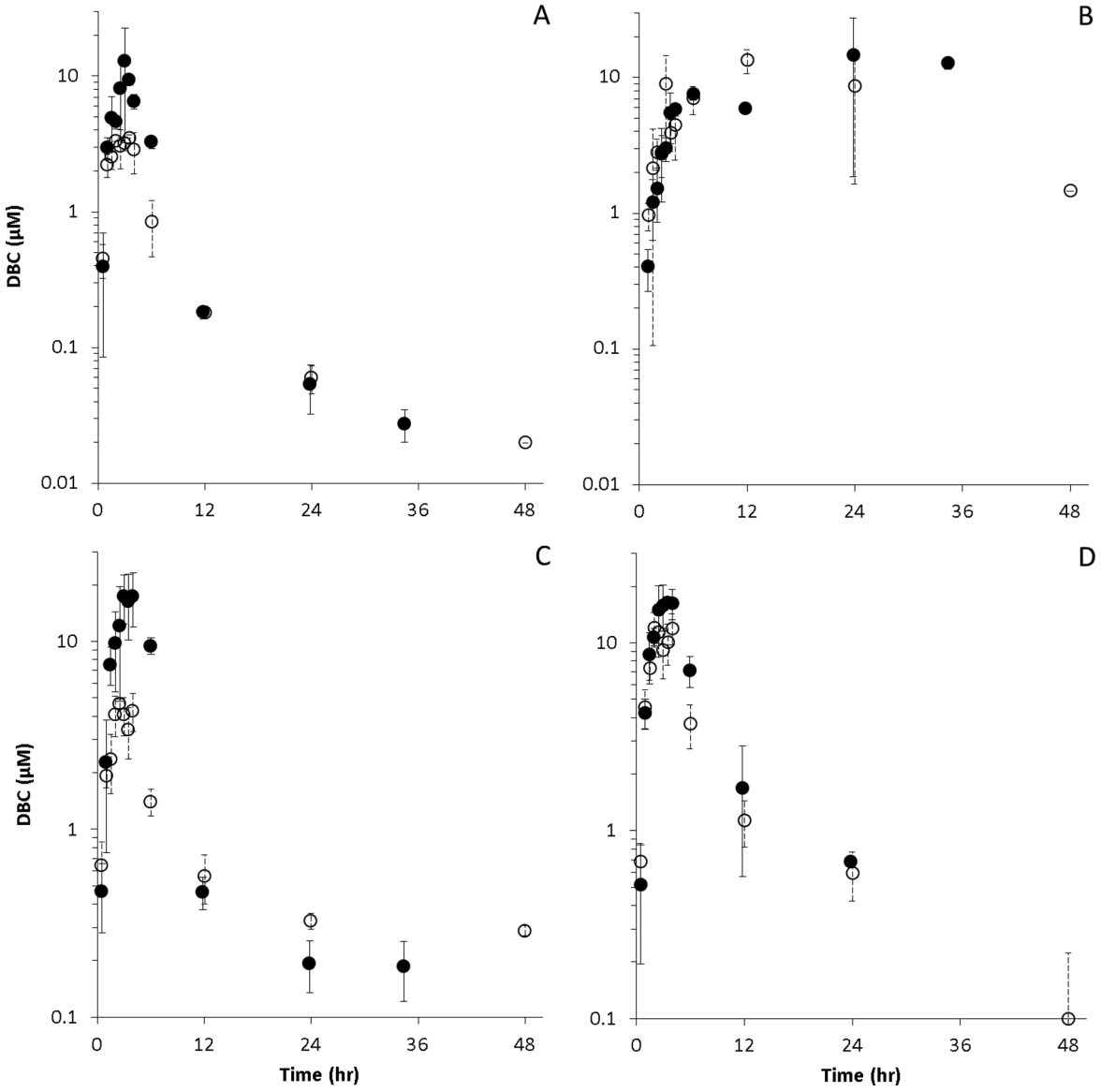

FIG. 4. DBC (μM) in blood and tissues of naïve (○) and pregnant (●) B6C129SF1/J mice administered bolus doses of 15 mg/kg DBC in corn oil via oral gavage. (A) Blood, (B) fat, (C) liver, and (D) lung.

were much higher than those in blood (16-fold higher in naïve mice; 9-fold higher in pregnant mice), as were the AUCs (approximately fourfold higher in both naïve and pregnant mice).

Tissues related to pregnancy: placenta and fetus. The pharmacokinetics of DBC and its hydroxylated metabolites in placenta and whole fetuses appear in Figure 7, and pharmacokinetic analyses appear in Tables 4 and 5. Tetraol metabolites were below limits of quantitation in these tissues. Peak concentrations of DBC occurred at 3 h in placenta and 4 h in fetuses, whereas DBC-11,12-diol peaked at 6 h in both. DBC concentrations were 10-fold higher in placenta than in fetus (5.2 vs. 0.57μM), whereas DBC-11,12-diol was roughly twofold higher (0.36 vs. 0.16μM). Figure 7 (panels C and D) shows the ratios of placental and fetal DBC and DBC-11,12-diol to those in maternal blood. Concentrations of DBC in placenta were generally comparable with maternal blood, whereas DBC-11,12-diol was elevated two- to fourfold. Fetal concentrations of DBC were 1–100× lower than those in maternal blood, whereas DBC-11,12-diol concentrations were comparable or even elevated compared with maternal blood.

There were no apparent differences between whole fetal concentrations based on AHR-responsive genotype, so data shown are for all fetuses combined at each time point.

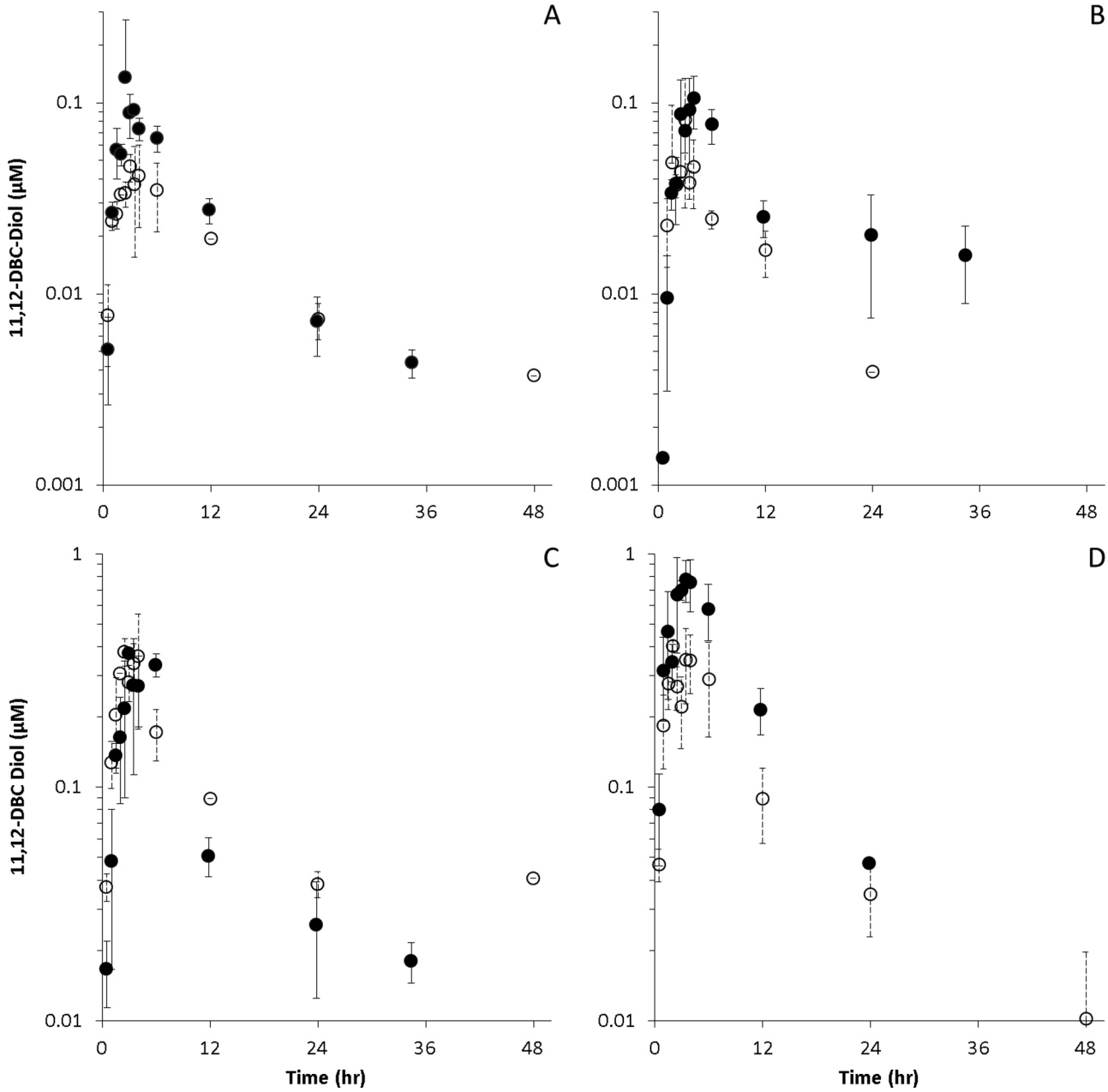

FIG. 5. DBC-11,12-diol (µM) in blood and tissues of naïve (○) and pregnant (●) B6C129SF1/J mice administered bolus doses of 15 mg/kg DBC in corn oil via oral gavage. (A) Blood, (B) fat, (C) liver, and (D) lung.

PBPK Model Simulations

To explore the observed differences in pharmacokinetics between pregnant and naïve mice, we extended our previous PBPK model for DBC to include physiological changes and additional compartments (e.g., fetuses and placenta) associated with pregnancy. Simulations of a 15 mg/kg DBC exposure in blood and liver of naïve and pregnant mice appear in Figure 8. Changes in physiology and tissue compartment size due to pregnancy resulted in a small increase in predicted blood concentrations (as illustrated by comparisons of AUC and/or C_{MAX}, Tables 4–6) but did not approach the nearly fourfold elevation of DBC concentrations observed in blood of pregnant mice; there was no discernible effect to predicted liver concentrations. However, by ABPP, we observed a 2- to 10-fold reduction in activity of many P450s and other enzymes relevant to PAH metabolism due to pregnancy (Table 7). Although a 5.6-fold reduction in activity was observed for CYP1A1, no activity was measured for CYP1B1 in naïve or pregnant mice. By applying the average 3.7-fold reduction to the maximum metabolic rates used in the model for the initial step in the metabolism of

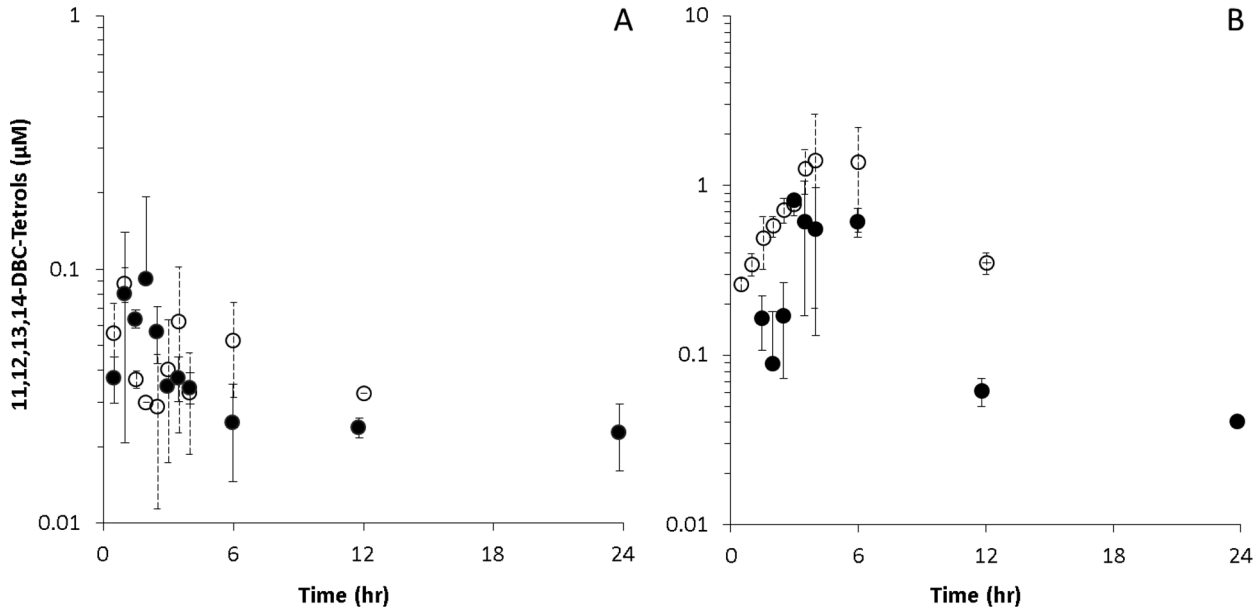

FIG. 6. DBC-11,12,13,14-tetraols (μM) in blood and tissues of naïve (○) and pregnant (●) B6C129SF1/J mice administered bolus doses of 15 mg/kg DBC in corn oil via oral gavage. (A) Blood and (B) liver.

DBC by P450s, the resulting prediction of DBC levels in blood and liver more closely resembled observed peak concentration data. The clearance of DBC from blood and liver remains much faster than the revised model predicts, similar to the simulations of nonpregnant mice.

DISCUSSION

The data presented here underscore the striking differences in the pharmacokinetics of orally administered DBC in naïve and pregnant mice. Concentrations of DBC and its hydroxylated metabolites were markedly higher in blood and tissues of pregnant animals. Because DBC is a highly potent carcinogen capable of crossing the placental barrier (Castro *et al.*, 2008b; Shorey *et al.*, 2012; Yu *et al.*, 2006), understanding the determinants of the observed differences in pharmacokinetics is of critical importance to defining risks to the pregnant animal and developing fetuses, as well as for extrapolation to relevant human exposures in the future.

Although our existing PBPK model for DBC (Crowell *et al.*, 2011) adequately described the pharmacokinetics of DBC in adult female mice, the model consistently underpredicted the blood and tissue pharmacokinetic data in pregnant mice even with the inclusion of physiological changes associated with pregnancy (e.g., increased compartment volume, blood flow, addition of placental and fetal compartments). We therefore evaluated a variety of other physiological and biochemical features that could plausibly underlie the observed pharmacokinetic differences. For example, slower gut transit times and greater relaxation of the intestines have been observed in rodents as well as humans, which could affect bioavailability of drugs or chemicals (Chang *et al.*, 1995, 1998; Pavek *et al.*, 2009; Shah *et al.*, 2000). However, the total percent of administered dose of DBC that was accounted for in the intestine and feces of naïve (8.7%) and pregnant mice (6.1%) at the end of each study suggests that overall bioavailability was not affected. Pharmacokinetic studies employing iv dosing would facilitate the isolation of GI absorption and transit effects from clearance processes that occur simultaneously with oral gavage administration. However, the very low solubility of DBC in aqueous vehicles makes this route of administration challenging. High concentrations of DBC-11,12-diol and DBC-11,12,13,14-tetraols in GI tissue relative to other tissues may be indicative of local metabolism, which is not currently included in the model but should be considered in the future.

Changes in blood chemistry may also affect binding and partitioning, and therefore systemic distribution, as has been observed for other chemicals (Lowe *et al.*, 2009; Pavek *et al.*, 2009). During late gestation, maternal serum protein levels have been observed to decrease, whereas blood lipids increase markedly (McMullin *et al.*, 2008). For both pregnant and naïve animals, our PBPK model relies on standard adult rodent blood and tissue chemistry for estimates of partitioning (Poulin and Theil, 2000) and uses an estimated fractional binding term to describe additional sequestration of DBC in the blood compartment (Crowell *et al.*, 2011). Due to the experimental challenges associated with such highly lipophilic, nonvolatile chemicals

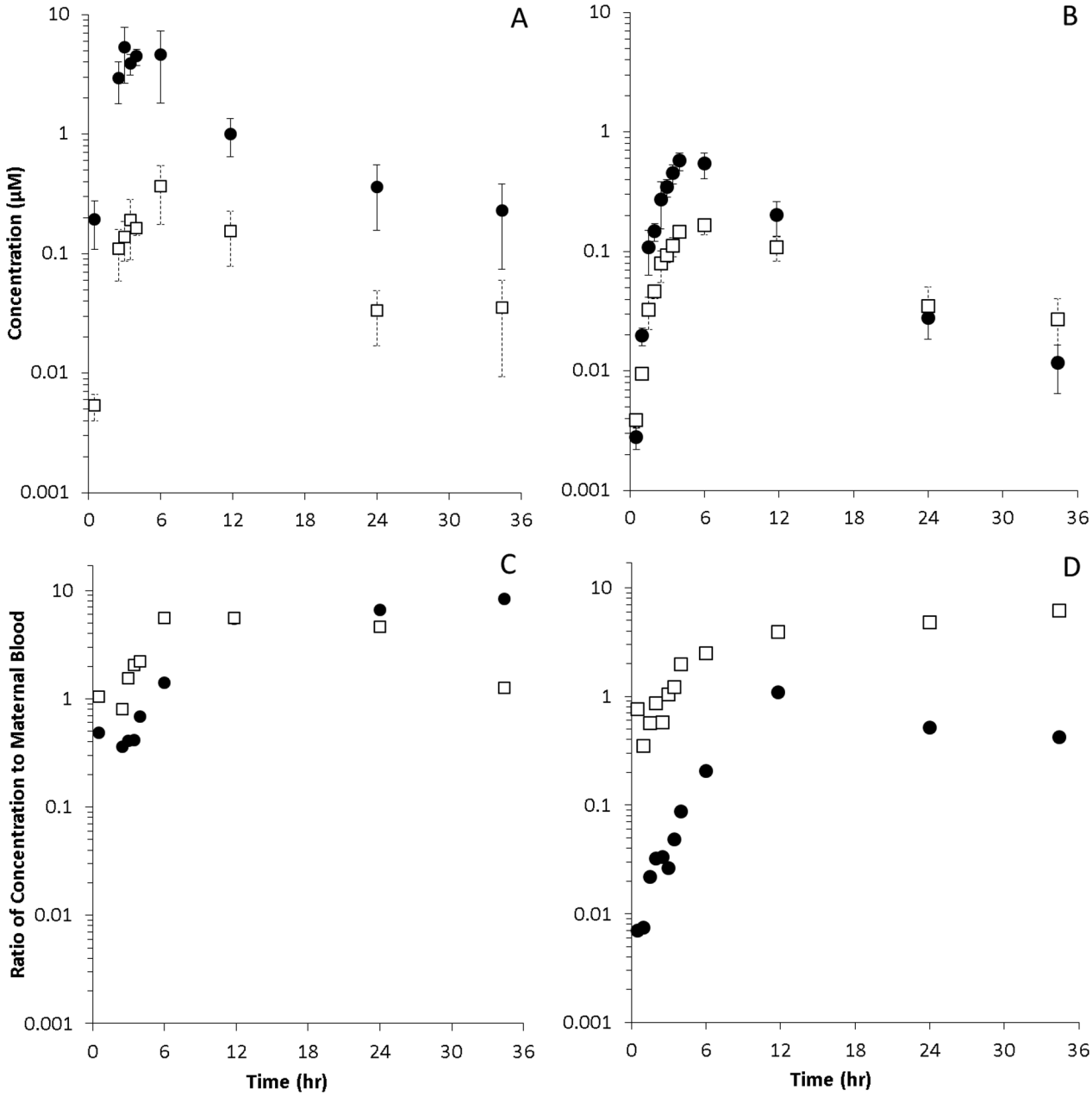

FIG. 7. DBC (●) and DBC-11,12-diol (□) in placentas (A and C) and whole fetuses (B and D). (A and B) Concentration (μM). (C and D) Ratio of tissue concentration to concentration in maternal blood (unitless).

as DBC and its metabolites and their affinity for plastic materials, traditional approaches for measurement of partitioning and binding are not tenable. However, more accurate descriptions of blood and tissue compositions in this strain of mice during late pregnancy could improve estimates of these biochemical parameters if such data become available.

Ultimately, changes in metabolism due to pregnancy were considered the most likely and readily verifiable source for the pharmacokinetic differences that were observed in this study. While gene expression, total P450 content and drug-metabolizing activities in the livers of rats have been observed to decrease (Dean and Stock, 1975; He *et al.*, 2005), no information on pregnancy-related enzyme activities were available for the B6129SF1/J mice used in these or the prior carcinogenicity studies. As a result, we applied an ABPP approach to evaluate changes in relative activities of 35 hepatic microsomal P450 enzymes, many of which are involved in PAH metabolism, due to pregnancy. ABPP is a chemoproteomic approach that facilitates the simultaneous comparison of multiple P450 enzyme activities through direct

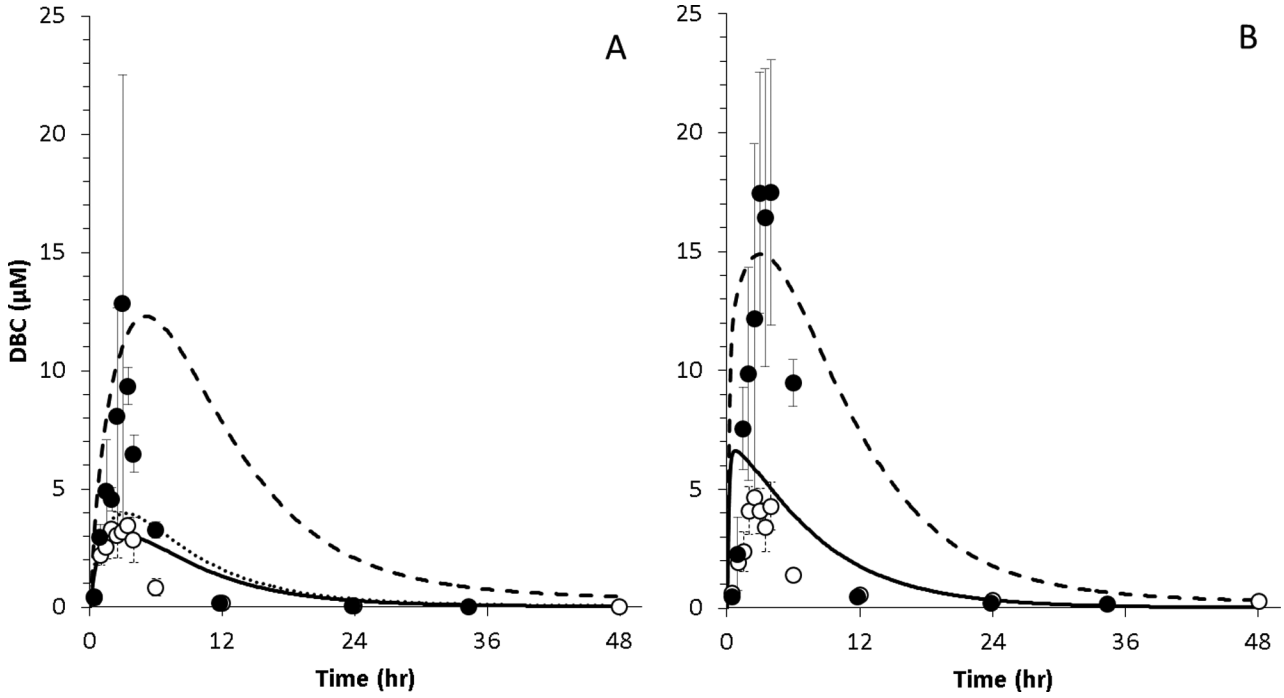

FIG. 8. Data (symbols) and PBPK model simulations (lines) of DBC in blood (A) and liver (B) of naïve (○, ····) and pregnant (●, –) B6C129SF1/J mice administered bolus doses of 15 mg/kg DBC in corn oil via oral gavage. A fourfold decrease in maximum hepatic metabolic rates measured by ABPP improved model predictions (---) compared with metabolic rates measured in nonpregnant animals.

measurement with arylalkyne or aliphatic alkyne containing chemical probes (Wright *et al.*, 2009). Arylalkyne and aliphatic alkynes are known to be mechanism-based inhibitors of P450 enzymes (Hollenberg *et al.*, 2008); therefore, our probes are oxidized directly in a NADPH-dependent manner by cytochrome P450s to yield a reactive ketene moiety. The electrophilic ketene then reacts with a nucleophilic amino acid residue within the active site of the P450, providing a covalent handle for downstream analyses. Via copper-catalyzed click chemistry, fluorescent reporters for gel imaging or biotin for enrichment and LC-MS analysis can be readily appended to probe-labeled P450 enzymes. Because this method involves measuring posttranslational enzyme activity rather than simple gene expression or protein abundance levels, it gives a more realistic description of the metabolic capabilities of an organism under specific conditions. Here, we have measured differences in enzyme activity between naïve and pregnant B6129SF1/J mice and found a 2- to 10-fold reduction in activities of over 30 P450s in the livers of pregnant mice (Table 7). Incorporating an overall average of fourfold reduction in V_{MAX} for the P450-dependent metabolism of DBC into the PBPK model dramatically improved model predictions of peak blood and liver concentrations in the pregnant animal although clearance of DBC remains faster than the model predicts (as was the case for naïve mice).

Although a reduction in CYP1A1 activity in pregnant mice was detected with ABPP, no activity was detected for CYP1B1 in liver tissue from naïve or pregnant mice. CYP1B1 is not constitutively expressed in liver but is inducible by aryl hydrocarbon receptor agonists over a time course relevant to the duration of this study. It has been suggested that CYP1B1 plays an important role in mediating the carcinogenicity of DBC in adult mice (Buters *et al.*, 2002; Castro *et al.*, 2008a), but whether CYP1B1 contributes significantly to systemic clearance or activation of DBC is unclear. ABPP probes have been previously shown to be active against human CYP1B1 (Wright *et al.*, 2009) but have not been extensively tested against mouse CYP1B1. Additional probe development as well as a more comprehensive assessment of enzyme activity in extrahepatic tissues, including lung and thymus, and during critical life stages, including fetal and neonatal development, are currently underway and may clarify this finding. Furthermore, we are pursuing traditional approaches, including measurement of global protein expression and purified enzyme assays, to provide additional context and detail for initial ABPP results, and guide the use of these results in PBPK model development and application.

As suggested by prior studies with ^{14}C-labeled DBC (Shorey *et al.*, 2012), we detected DBC and its metabolites in the fetal compartment. We did not observe variations in the pharmacokinetics between fetal AHR-responsive and nonresponsive genotypes at the whole fetal level, although differences may exist in individual tissues, a possibility we are currently investigating. Although fetal concentrations of DBC were low relative to maternal blood, DBC-11,12-diol concentrations were elevated, a finding that suggests

TABLE 7
Reduction (Fold Change) in P450 Enzyme Activities in Pregnant Versus Naïve Mice

	Naïve vs. pregnant
Enzyme	Fold difference
CYP17A1	0.35
CYP1A1	5.62
CYP1A2	5.37
CYP2C37	8.43
CYP2C38	2.86
CYP2C39	2.00
CYP2C40	2.90
CYP2C54	5.97
CYP2C70	1.30
CYP27A1	4.63
CYP2A4	2.39
CYP2A5	2.40
CYP 2A12	2.21
CYP2B9	5.71
CYP2B10	1.94
CYP2B19	5.44
CYP2C29	2.15
CYP2D9	1.43
CYP2D10	1.34
CYP2D11	1.42
CYP2D26	1.33
CYP2E1	6.58
CYP2F2	4.79
CYP2J5	1.48
CYP2J6	1.49
CYP3A41	0.96
CYP3A11	1.71
CYP3A13	1.81
CYP3A16	1.37
CYP3A25	0.59
CYP4A10	—
CYP4A14	30.05
CYP4A12A	—
CYP4F14	4.34
CYP51A1	1.18
Average change	3.74 ± 5.1

the possibility of fetal metabolism, or more efficient partitioning or transport of the diol metabolite across the placenta. As in adult mice, previous studies have shown that susceptibility of offspring to DBC-induced carcinogenesis is dependent on CYP1B1 metabolism in addition to AHR-responsive phenotypes following maternal DBC exposure (Castro *et al.*, 2008a). Although fetal metabolism appears to play a role in the carcinogenic mechanism of action and the higher DBC-diol metabolite levels we observed, it is unclear from the present data whether fetal enzyme activities alone are sufficient to local fetal kinetics. In addition to fetal tissue-specific pharmacokinetics, fetal tissue metabolic capacities are currently being assessed by ABPP in ongoing pharmacokinetic studies and an enzyme ontogeny study in mouse and human fetal and neonatal tissues.

Currently, our focus has been on the impact of pregnancy on the pharmacokinetics of DBC in the adult mouse; however, the more vulnerable target is of course the developing fetus. As we complete subsequent pharmacokinetic studies, including individual fetal tissues, the PBPK model will be expanded to allow closer inspection of pharmacokinetics and other processes influencing the fate of DBC and its metabolites in target tissues for this sensitive population that can be translated into future human health risk assessments.

FUNDING

National Institute of Environmental Health Sciences (P42 ES016465), National Institute of General Medical Sciences (8P41GM103493-10), United States Department of Energy Laboratory Directed Research and Development Project 90001.

REFERENCES

Aarstad, K., Toftgard R. and Nilsen O. G. (1987). "A Comparison of the binding and distribution of benzo[a]pyrene in human and rat serum." *Toxicology* **47(3),** 235–245.

Ansong, C., Ortega, C., Payne, S. H., Haft, D. H., Chauvignè-Hines, L. M., Lewis, M. P., Ollodart, A. R., Purvine, S. O., Shukla, A. K., Fortuin, S., *et al.* (2013). Identification of widespread adenosine nucleotide binding in Mycobacterium tuberculosis. *Chem. Biol*. **20,** 123–133.

Brown, R. P., Delp, M. D., Lindstedt, S. L., Rhomberg, L. R., and Beliles, R. P. (1997). Physiological parameter values for physiologically based pharmacokinetic models. *Toxicol. Ind. Health* **13,** 407–484.

Buesen, R., Mock, M., Seidel, A., Jacob, J., and Lampen, A. (2002). Interaction between metabolism and transport of benzo[a]pyrene and its metabolites in enterocytes. *Toxicol. Appl. Pharmacol*. **183,** 168–178.

Buters, J. T., Mahadevan, B., Quintanilla-Martinez, L., Gonzalez, F. J., Greim, H., Baird, W. M., and Luch, A. (2002). Cytochrome P450 1B1 determines susceptibility to dibenzo[a,l]pyrene-induced tumor formation. *Chem. Res. Toxicol*. **15,** 1127–1135.

Castro, D. J., Baird, W. M., Pereira, C. B., Giovanini, J., Löhr, C. V., Fischer, K. A., Yu, Z., Gonzalez, F. J., Krueger, S. K., and Williams, D. E. (2008a). Fetal mouse Cyp1b1 and transplacental carcinogenesis from maternal exposure to dibenzo(a,l)pyrene. *Cancer Prev. Res. (Phila)*. **1,** 128–134.

Castro, D. J., Löhr, C. V., Fischer, K. A., Pereira, C. B., and Williams, D. E. (2008b). Lymphoma and lung cancer in offspring born to pregnant mice dosed with dibenzo[a,l]pyrene: The importance of in utero vs. lactational exposure. *Toxicol. Appl. Pharmacol*. **233,** 454–458.

Cavalieri, E. L., Higginbotham, S., RamaKrishna, N. V., Devanesan, P. D., Todorovic, R., Rogan, E. G., and Salmasi, S. (1991). Comparative dose-response tumorigenicity studies of dibenzo[alpha,l]pyrene versus 7,12-dimethylbenz[alpha]anthracene, benzo[alpha]pyrene and two dibenzo[alpha,l]pyrene dihydrodiols in mouse skin and rat mammary gland. *Carcinogenesis* **12,** 1939–1944.

Cavalieri, E. L., Rogan, E. G., Higginbotham, S., Cremonesi, P., and Salmasi, S. (1989). Tumor-initiating activity in mouse skin and carcinogenicity in rat mammary gland of dibenzo[a]pyrenes: The very potent environmental carcinogen dibenzo[a, l]pyrene. *J. Cancer Res. Clin. Oncol*. **115,** 67–72.

Chang, F. Y., Lee, S. D., Yeh, G. H., Lu, C. C., Wang, P. S., and Wang, S. W. (1998). Disturbed small intestinal motility in the late rat pregnancy. *Gynecol. Obstet. Invest*. **45,** 221–224.

Chang, F. Y., Lee, S. D., Yeh, G. H., and Wang, P. S. (1995). Influence of pregnancy and uterine weight on rat gastrointestinal transit. *J. Gastroenterol. Hepatol*. **10,** 585–588.

Crowell, S. R., Amin, S. G., Anderson, K. A., Krishnegowda, G., Sharma, A. K., Soelberg, J. J., Williams, D. E., and Corley, R. A. (2011). Preliminary physiologically based pharmacokinetic models for benzo[a]pyrene and dibenzo[def,p]chrysene in rodents. *Toxicol. Appl. Pharmacol*. **257,** 365–376.

Dean, M. E., and Stock, B. H. (1975). Hepatic microsomal metabolism of drugs during pregnancy in the rat. *Drug Metab. Dispos*. **3,** 325–331.

Guengerich, F. P. (1994). Analysis and Characterization of Enzymes. *Principles and methods of toxicology*. A. W. Hayes. New York, Raven Press: 1259–1314.

He, X. J., Ejiri, N., Nakayama, H., and Doi, K. (2005). Effects of pregnancy on CYPs protein expression in rat liver. *Exp. Mol. Pathol*. **78,** 64–70.

Higginbotham, S., RamaKrishna, N. V., Johansson, S. L., Rogan, E. G., and Cavalieri, E. L. (1993). Tumor-initiating activity and carcinogenicity of dibenzo[a,l]pyrene versus 7,12-dimethylbenz[a]anthracene and benzo[a] pyrene at low doses in mouse skin. *Carcinogenesis* **14,** 875–878.

Hollenberg, P. F., Kent, U. M., and Bumpus, N. N. (2008). Mechanism-based inactivation of human cytochromes p450s: Experimental characterization, reactive intermediates, and clinical implications. *Chem. Res. Toxicol*. **21,** 189–205.

IARC. (2010). Some non-heterocyclic polycyclic aromatic hydrocarbons and some related exposures. IARC Monographs on the Evaluation of Carcinogenic Risks to Humans. International Agency for Research on Cancer, Lyon, France.

Kim, S., Gupta, N., and Pevzner, P. A. (2008). Spectral probabilities and generating functions of tandem mass spectra: A strike against decoy databases. *J. Proteome Res*. **7,** 3354–3363.

Krzeminski, J., Lin, J. M., Amin, S., and Hecht, S. S. (1994). Synthesis of Fjord region diol epoxides as potential ultimate carcinogens of dibenzo[a,l]pyrene. *Chem. Res. Toxicol*. **7,** 125–129.

LaVoie, E. J., He, Z. M., Meegalla, R. L., and Weyand, E. H. (1993). Exceptional tumor-initiating activity of 4-fluorobenzo[j]-fluoranthene on mouse skin: Comparison with benzo[j]-fluoranthene, 10-fluoro-benzo[j]fluoranthene, benzo[a]pyrene, dibenzo[a,l]pyrene and 7,12-dimethylbenz[a]anthracene. *Cancer Lett*. **70,** 7–14.

Lowe, E. R., Poet, T. S., Rick, D. L., Marty, M. S., Mattsson, J. L., Timchalk, C., and Bartels, M. J. (2009). The effect of plasma lipids on the pharmacokinetics of chlorpyrifos and the impact on interpretation of blood biomonitoring data. *Toxicol. Sci*. **108,** 258–272.

Luch, A., Platt, K. L., and Seidel, A. (1998). Synthesis of fjord region tetraols and their use in hepatic biotransformation studies of dihydrodiols of benzo[c] chrysene, benzo[g]chrysene and dibenzo[a,l]pyrene. *Carcinogenesis* **19,** 639–648.

McMullin, T. S., Lowe, E. R., Bartels, M. J., and Marty, M. S. (2008). Dynamic changes in lipids and proteins of maternal, fetal, and pup blood and milk during perinatal development in CD and Wistar rats. *Toxicol. Sci*. **105,** 260–274.

NIH. (2011). *Guide for the Care and Use of Laboratory Animals*. National Research Council, Washington, DC.

Oflaherty, E. J., Scott, W., Schreiner C., and Beliles R. P. (1992). "A PHYSIOLOGICALLY BASED KINETIC-MODEL OF RAT AND MOUSE GESTATION - DISPOSITION OF A WEAK ACID." *Toxicology and Applied Pharmacology* **112(2),** 245–256.

Osinski, M. A., Seifert, T. R., Cox, B. F., and Gintant G. A. (2002). "An improved method of evaluation of drug-evoked changes in gastric emptying in mice." *Journal of Pharmacological and Toxicological Methods* **47(2),** 115–120.

Pavek, P., Ceckova, M., and Staud, F. (2009). Variation of drug kinetics in pregnancy. *Curr. Drug Metab*. **10,** 520–529.

Platt, K. L., Dienes, H. P., Tommasone, M., and Luch, A. (2004). Tumor formation in the neonatal mouse bioassay indicates that the potent carcinogen dibenzo[def,p]chrysene (dibenzo[a,l]pyrene) is activated in vivo via its trans-11,12-dihydrodiol. *Chem. Biol. Interact*. **148,** 27–36.

Polpitiya, A. D., Qian, W. J., Jaitly, N., Petyuk, V. A., Adkins, J. N., Camp, D. G., II, Anderson, G. A., and Smith, R. D. (2008). DAnTE: A statistical tool for quantitative analysis of -omics data. *Bioinformatics* **24,** 1556–1558.

Poulin, P., and Theil, F. P. (2000). A priori prediction of tissue:plasma partition coefficients of drugs to facilitate the use of physiologically-based pharmacokinetic models in drug discovery. *J. Pharm. Sci*. **89,** 16–35.

Prahalad, A. K., Ross, J. A., Nelson, G. B., Roop, B. C., King, L. C., Nesnow, S., and Mass, M. J. (1997). Dibenzo[a,l]pyrene-induced DNA adduction, tumorigenicity, and Ki-ras oncogene mutations in strain A/J mouse lung. *Carcinogenesis* **18,** 1955–1963.

Shah, S., Hobbs, A., Singh, R., Cuevas, J., Ignarro, L. J., and Chaudhuri, G. (2000). Gastrointestinal motility during pregnancy: Role of nitrergic component of NANC nerves. *Am. J. Physiol. Regul. Integr. Comp. Physiol*. **279,** R1478–R1485.

Sharma, A. K., Kumar, S., and Amin, S. (2004). A highly abbreviated synthesis of dibenzo[def,p]chrysene and Its 12-methoxy derivative, a key precursor for the synthesis of the proximate and ultimate carcinogens of dibenzo[def,p] chrysene. *J. Org. Chem*. **69,** 3979–3982.

Shorey, L. E., Castro, D. J., Baird, W. M., Siddens, L. K., Löhr, C. V., Matzke, M. M., Waters, K. M., Corley, R. A., and Williams, D. E. (2012). Transplacental carcinogenesis with dibenzo[def,p]chrysene (DBC): Timing of maternal exposures determines target tissue response in offspring. *Cancer Lett*. **317,** 49–55.

Speers, A. E., Adam, G. C., and Cravatt, B. F. (2003). Activity-based protein profiling in vivo using a copper(i)-catalyzed azide-alkyne [3 + 2] cycloaddition. *J. Am. Chem. Soc*. **125,** 4686–4687.

Staats, D. A., Fisher, J. W., and Connolly, R. B. (1991). Gastrointestinal absorption of xenobiotics in physiologically based pharmacokinetic models. A two-compartment description. *Drug Metab. Dispos*. **19,** 144–148.

Stanley, J. R., Adkins, J. N., Slysz, G. W., Monroe, M. E., Purvine, S. O., Karpievitch, Y. V., Anderson, G. A., Smith, R. D., and Dabney, A. R. (2011). A statistical method for assessing peptide identification confidence in accurate mass and time tag proteomics. *Anal. Chem*. **83,** 6135–6140.

Walker, N. J., Gastel, J. A., Costa, L. T., Clark, G. C., Lucier, G. W., and Sutter, T. R. (1995). Rat CYP1B1: An adrenal cytochrome P450 that exhibits sex-dependent expression in livers and kidneys of TCDD-treated animals. *Carcinogenesis* **16,** 1319–1327.

Wright, A. T., and Cravatt, B. F. (2007). Chemical proteomic probes for profiling cytochrome p450 activities and drug interactions in vivo. *Chem. Biol*. **14,** 1043–1051.

Wright, A. T., Song, J. D., and Cravatt, B. F. (2009). A suite of activity-based probes for human cytochrome P450 enzymes. *J. Am. Chem. Soc*. **131,** 10692–10700.

Xue, W., and Warshawsky, D. (2005). Metabolic activation of polycyclic and heterocyclic aromatic hydrocarbons and DNA damage: A review. *Toxicol. Appl. Pharmacol*. **206,** 73–93.

Yates, J. R., III, Eng, J. K., McCormack, A. L., and Schieltz, D. (1995). Method to correlate tandem mass spectra of modified peptides to amino acid sequences in the protein database. *Anal. Chem*. **67,** 1426–1436.

Yu, Z., Loehr, C. V., Fischer, K. A., Louderback, M. A., Krueger, S. K., Dashwood, R. H., Kerkvliet, N. I., Pereira, C. B., Jennings-Gee, J. E., Dance, S. T., *et al.* (2006). In utero exposure of mice to dibenzo[a,l]pyrene produces lymphoma in the offspring: Role of the aryl hydrocarbon receptor. *Cancer Res*. **66,** 755–762.

Zhang, Q. Y., Dunbar, D., and Kaminsky, L. S. (2003). Characterization of mouse small intestinal cytochrome P450 expression. *Drug Metab. Dispos*. **31,** 1346–1351.

Zimmer, J. S., Monroe, M. E., Qian, W. J., and Smith, R. D. (2006). Advances in proteomics data analysis and display using an accurate mass and time tag approach. *Mass Spectrom. Rev*. **25,** 450–482.